

Quantum pumping with adiabatically modulated barriers in three-band pseudospin-1 Dirac-Weyl systems

Xiaomei Chen and Rui Zhu^{*}

*Department of Physics, South China University of Technology,
Guangzhou 510641, People's Republic of China*

Abstract

In this work, pumped currents of the adiabatically-driven double-barrier structure based on the pseudospin-1 Dirac-Weyl fermions are studied. As a result of the three-band dispersion and hence the unique properties of pseudospin-1 Dirac-Weyl quasiparticles, sharp current-direction reversal is found at certain parameter settings especially at the Dirac point of the band structure, where apexes of the two cones touches at the flat band. Such a behavior can be interpreted consistently by the Berry phase of the scattering matrix and the classical turnstile mechanism.

PACS numbers: 72.10.Bg, 73.23.-b, 02.40.Pc

arXiv:1812.00496v1 [cond-mat.mes-hall] 3 Dec 2018

^{*} Corresponding author. Electronic address: rzhu@scut.edu.cn

I. INTRODUCTION

After quantized particle transport driven by adiabatic cyclic potential variation was proposed by D. J. Thouless in 1983¹, such a concept has attracted unceasing interest in the physical society concerning its theoretical meaning and potential applications in various fields such as a precision current standard and neural networks²⁻⁴. Mechanism of the quantum pump can be interpreted consistently by the Berry phase of the scattering matrix in the parameter space within the modulation cycle² and the classic turnstile picture^{5,6}. Usually, the pumped current is unidirectional when the phase difference between the two driving parameters is fixed. In the turnstile picture, the opening order of the two gates is defined by the driving phase. The first-opened gate let in the particle and the second-opened gate let it out forming a dc current after a cycle is completed. However, reversed dc current direction has been discovered in various systems even when the driving phase is fixed such as in monolayer graphene⁶ and carbon nanotube-superconductor hybrid systems⁷. This is because that conventionally a “gate” is defined by a potential barrier and higher barriers allow smaller transmission probabilities. However, as a result of the Klein tunneling effect, the potential barrier becomes transparent regardless of its height at certain parameter settings. When higher barrier allows even stronger transmission, the opening and closing of a “gate” in the quantum pump is reversed and so the driven current is reversed with the driving phase difference unchanged. The same phenomenon is also discovered in the superconductive carbon nanotube when Andreev reflection again violates the higher-barrier-lower-transmission convention and reversed the pumped current under the same driving forces. This turnstile interpretation of the reversed pumped current coincides with the Berry phase of the scattering matrix in the parameter space within the modulation cycle. However, a clear comparison between the two mechanisms is lacking, which is one of the motivations of this work.

After the idea of the adiabatic quantum pump (also called Thouless pump and parametric pump) is proposed, such a mechanism has been investigated in various transport devices such as a single spin in diamond⁸, quantum-dot structures⁹, Rashba nanowires¹⁰, MachZehnder interferometers¹¹, the magnetic nanowire with double domain walls¹², magnetic-barrier-modulated two dimensional electron gas¹³, mesoscopic rings with Aharonov-Casher and Aharonov-Bohm effect¹⁴, magnetic tunnel junctions¹⁵, and monolayer graphene^{6,16}. Correspondingly, theoretical techniques have been put forward for the treatment of the quantum

pumps such as the scattering matrix formalism¹⁷, non-equilibrium Green's function¹⁸⁻²¹, and the quantum master equation approach⁹. In this work, we use the scattering matrix approach for ac transport, which defines the Berry phase formed within the looped trajectory of the two varying parameters^{2,17,22}.

Recently, after realization of the monolayer graphene, which is characterized as a pseudospin-1/2 Dirac-Weyl fermionic material, a family of general pseudospin- s ($s = 1/2, 1, 3/2, \dots$) Dirac-Weyl fermionic materials has been proposed by sharing similar band structure with one or several pairs of Dirac cones. Pseudospin-1 materials with band structure of two Dirac cones and a flat band through where the cones intersect have attracted intense interest in the physical society currently. Numerical or experimental studies have proposed various host material of such band structure such as conventional crystal with special space group symmetries^{23,24}, in the electronic, photonic, and phononic Lieb lattice²⁵⁻³⁰, kagome lattice³⁰, dice or T_3 lattice³⁰⁻³³, and K_4 crystal³⁴. Along with these progress in material building, various transport properties of the pseudospin-1 Dirac-Weyl fermions have been investigated such as super Klein tunneling effect^{35,36}, magneto-optics³⁷, Hall quantization³⁸, and Hofstadter butterfly³⁹ in a magnetic field. While the adiabatic quantum pumping process serves as an important platform to detect various properties of novel quantum states, it is worthwhile to apply the idea on newly-emerged pseudospin-1 Dirac-Weyl materials. To understand how their particular transport property modify the adiabatically-driven pumped current is the other motivation of this work.

The plan of the present work is as follows. In Sec. 2, the model is introduced and the key formulas for the scattering matrix, Berry phase, and pumped current are given. In Sec. 3, we present numerical results of the pumped current and discussions of the underlying mechanisms. In Sec. 4, a rigorous proof of the consistency between the quantum Berry phase picture and the classic turnstile mechanism for adiabatic quantum pumping is provided. A brief summary is given in Sec. 5.

II. MODEL AND FORMALISM

We consider a two-dimensional (2D) non-interacting pseudospin-1 Dirac-Weyl system modulated by two time-dependent electric potential barriers illustrated in Fig. 1. The pseudospin-1 Dirac-Weyl fermions are charged quasiparticles originating from free electrons

moving in the three-band structure consisting of gapless tip-to-tip two cones intersected by a flat band, which is shown in Fig. 1 (c). Their dynamics is governed by the dot product of the spin-1 operator and the momentum. Matrices of the spin-1 operator $\hat{S} = (\hat{S}_x, \hat{S}_y, \hat{S}_z)$ in the \hat{S}_z -representation (the representation that \hat{S}_z is diagonalized) can be deduced from spin-lifting/lowering operators $\hat{S}_\pm = \hat{S}_x \pm \hat{S}_y$ by $\hat{S}_\pm |S, S_z\rangle = \sqrt{(S \mp S_z)(S \pm S_z + 1)} |S, S_z \pm 1\rangle$ ⁴⁰. Simple algebra leads to the results that

$$\hat{S}_x = \frac{1}{\sqrt{2}} \begin{pmatrix} 0 & 1 & 0 \\ 1 & 0 & 1 \\ 0 & 1 & 0 \end{pmatrix}, \quad \hat{S}_y = \frac{1}{\sqrt{2}} \begin{pmatrix} 0 & -i & 0 \\ i & 0 & -i \\ 0 & i & 0 \end{pmatrix}, \quad \hat{S}_z = \begin{pmatrix} 1 & 0 & 0 \\ 0 & 0 & 0 \\ 0 & 0 & -1 \end{pmatrix}. \quad (1)$$

By applying ac gate voltages, Hamiltonian of the pseudospin-1 Dirac-Weyl fermions has the form

$$\hat{H} = -i\hbar v_g \hat{\mathbf{S}} \cdot \nabla + V(x, t), \quad (2)$$

where $\hat{\mathbf{S}}$ is the spin-1 operator defined in Eq. (1), $v_g \approx 10^6$ m/s is the group velocity associated with the slope of the Dirac cone. As shown in Fig. 1 (a), the potential function has the form

$$V(x, t) = \begin{cases} V_0 + V_1(t), & 0 < x < L_1, \\ V_0 + V_2(t), & L_2 < x < L_3, \\ 0, & \text{others,} \end{cases} \quad (3)$$

with $V_1(t) = V_{1\omega} \cos(\omega t + \varphi)$ and $V_2(t) = V_{2\omega} \cos(\omega t)$. The Fermi energy of the two reservoirs to the two sides of the double-barrier structure are equalized to eliminate the external bias and secure energy-conserved tunneling. While the frequency of the potential modulation ω is small compared to the carrier interaction time (Wigner delay time) with the conductor, the quantum pump can be considered ‘‘adiabatic’’^{1,17,22}. In this case, one can employ an instant scattering matrix approach, which depends only parametrically on the time t . The Wigner-Smith delay time can be evaluated by $\tau = \text{Tr}(-i\hbar \mathbf{s}^\dagger \frac{\partial \mathbf{s}}{\partial E_F})$, with \mathbf{s} the scattering matrix defined in Eq. (5). Calculations below show $\tau \approx 10^{-14}$ s for all the parameter values. So the adiabatic condition can be well justified when ω is in the order of MHz³.

For studying the transport properties, the flux normalized scattering modes in different

regions can be expressed in terms of the eigenspinors as

$$\Psi = \begin{pmatrix} \psi_1 \\ \psi_2 \\ \psi_3 \end{pmatrix} = \begin{cases} a_l \psi_{\rightarrow} + b_l \psi_{\leftarrow}, & x < 0, \\ a_1 \psi_{1\rightarrow} + b_1 \psi_{1\leftarrow}, & 0 < x < L_1, \\ a_2 \psi_{\rightarrow} + b_2 \psi_{\leftarrow}, & L_1 < x < L_2, \\ a_3 \psi_{2\rightarrow} + b_3 \psi_{2\leftarrow}, & L_2 < x < L_3, \\ a_r \psi_{\leftarrow} + b_r \psi_{\rightarrow}, & x > L_3, \end{cases} \quad (4)$$

where $k_x = \sqrt{E_F^2/(\hbar v_g)^2 - k_y^2}$ with E_F the quasiparticle energy at the Fermi level of the reservoirs. $\psi_{\rightarrow} = \frac{1}{2\sqrt{\cos\theta}}(e^{-i\theta}, \sqrt{2}s, e^{i\theta})^T e^{ik_x x}$ for $E_F \neq 0$ (quasiparticles on the two cone bands) and $\frac{1}{\sqrt{2}}(-e^{-i\theta}, 0, e^{i\theta})^T$ (we also identify it as ψ_0 for discussions in the next section) for $E_F = 0$ (quasiparticles on the flat band). $\theta = \arctan(k_y/k_x)$, and $s = \text{sgn}(E_F)$. ψ_{\leftarrow} can be obtained by replacing k_x with $-k_x$ in ψ_{\rightarrow} ; $\psi_{i\rightarrow}/\psi_{i\leftarrow}$ ($i = 1, 2$) can be obtained by replacing k_x with $q_{xi} = \sqrt{(E_F - V_0 - V_i)^2/(\hbar v_g)^2 - k_y^2}$ and s with $s'_i = \text{sgn}(E_F - V_0 - V_i)$ in $\psi_{\rightarrow}/\psi_{\leftarrow}$. The flux normalization factor $2\sqrt{\cos\theta}$ is obtained⁴¹ by letting $\Psi^\dagger(\partial\hat{H}/\partial k_x)\Psi = 1$. ψ_i ($i = 1, 2, 3$) picks up the i -th row of the spinor wave function in all the five regions. Note that quasiparticles on the flat band contribute no flux in the x -direction. However, it must be taken into account in the pumping mechanisms while the Fermi energy lies close to the Dirac point. We will go to this point again in the next section.

The boundary conditions are that $\psi_1 + \psi_3$ and ψ_2 are continuous at the interfaces respectively³⁵. After some algebra, the instant scattering matrix connecting the incident and outgoing modes can be expressed as

$$\begin{pmatrix} b_l \\ b_r \end{pmatrix} = \begin{pmatrix} r & t' \\ t & r' \end{pmatrix} \begin{pmatrix} a_l \\ a_r \end{pmatrix} = \mathbf{s}(V_1, V_2) \begin{pmatrix} a_l \\ a_r \end{pmatrix}, \quad (5)$$

where \mathbf{s} is parameter-dependent.

The dc pumped current flowing from the α reservoir at zero temperature could be expressed in terms of the Berry phase of the scattering matrix formed within the looped trajectory of the two varying parameters as^{2,17,22}

$$I_{p\alpha} = \frac{\omega e}{2\pi} \int_A \Omega(\alpha) dV_1 dV_2, \quad (6)$$

where

$$\Omega(\alpha) = \sum_{\beta} \text{Im} \frac{\partial s_{\alpha\beta}^*}{\partial V_1} \frac{\partial s_{\alpha\beta}}{\partial V_2}. \quad (7)$$

A is the enclosed area in the V_1 - V_2 parameter space. While the driving amplitude is small ($V_{i\omega} \ll V_0$), the Berry curvature can be considered uniform within A and we have

$$I_{p\alpha} = \frac{\omega e \sin \varphi V_{1\omega} V_{2\omega}}{2\pi} \Omega(\alpha). \quad (8)$$

Conservation of current flux secures that the pumped currents flowing from the left and right reservoirs are equal: $I_{pl} = I_{pr}$. The angle-averaged pumped current can be obtained as

$$I_{p\alpha T} = \int_{-\pi/2}^{\pi/2} I_{p\alpha} \cos \theta d\theta. \quad (9)$$

III. RESULTS AND DISCUSSIONS

Previously we know that transport properties of the pseudospin-1 Dirac-Weyl fermions differs from free electrons in two ways. One is super Klein tunneling, which gives perfect transmission through a potential barrier for all incident angles while the quasiparticle energy equals one half the barrier height³⁵. The other is particle-hole symmetry above and below the Dirac point of a potential barrier, which is a shared property with pseudospin-1/2 Dirac-Weyl fermions on monolayer graphene⁴². It gives that the transmission probability closely above and below the Dirac point is mirror symmetric because hole states with identical dispersion to electrons exist within the potential barrier unlike the potential barrier formed by the energy gap in semiconductor heterostructures. These two properties are demonstrated in the conductivity through a single potential barrier shown in Fig. 1 (d). As a result of super Klein tunneling, the conductivity shows a local maximum at the Fermi energy close to half the barrier height. Because the conductivity also depends on the velocity or Fermi wavevector of the charge carriers, the maximum is parabolically-shaped under the present parameter settings and occurs at the Fermi energy larger than half the barrier height. For higher potential barriers, the maximum can be a sharp Λ -shaped peak appearing at the Fermi energy equal half the barrier height⁴³. Because of the existence of the two maximum peaks in the single-barrier transmission probability and hence in the conductivity, it occurs that under certain conditions higher barrier allows larger quasiparticle transmission. The mechanisms of an adiabatic quantum pump in a mesoscopic system can be illustrated consistently by a classic turnstile picture and by the the Berry phase of the scattering matrix in the parameter space^{2,5,6}. The turnstile picture can be illustrated within the framework of the single electron approximation and coherent tunneling constrained by the Pauli principle. The two oscillating

potential barriers work like two “gates” in a real turnstile. Usually lower potential allows larger transmissivity and thus defines opening of one gate. When the two potentials oscillate with a phase difference, the two gates open one by one. Constrained by the Pauli principle, only one electron can occupy the inner single-particle state confined in the quantum well formed by the two potential barriers at one time, electrons flow in a direction determined by the driving phase difference. However, in monolayer graphene and in the pseudospin-1 Dirac-Weyl system, Klein tunneling, super Klein tunneling, and particle-hole symmetry at the Dirac point give rise to a reversal of the transmissivity-barrier height relation. As a result, direction of the dc pumped current is reversed.

Numerical results of the pumped current are shown in Fig. 2. It can be seen from Fig. 1 (d) that when the value of E_F is between 70 meV and 100 meV, conductivity through higher potential barriers is larger than that through lower barriers. Angular dependence of the pumped current at Fermi energies selected within this range is shown in Fig. 2 (b). With φ fixed at $\pi/2$, potential barrier V_1 starts lowering first and then it rises and V_2 starts lowering. Usually (like in a semiconductor heterostructure) higher potential barriers give rise to smaller transmission probability. The process can be interpreted as “gate” V_1 “opens” first allowing one particle to enter the middle single-particle state from the left reservoir and then it “closes” and “gate” V_2 “opens” allowing the particle to leave the device and enter the right reservoir. This completes a pump cycle and a dc current is generated. Such is the classical turnstile picture of the pumping mechanism. However, for pseudospin-1 Dirac-Weyl fermions higher potential barriers give rise to larger transmission probability under certain parameter settings as demonstrated in Fig. 1 (d). In the classical turnstile picture, this means that the definition of “opening” and “closing” of the “gate” is reversed. This is the reason for the negative (direction-reversed) pumped current shown in Fig. 2 (b).

It can also be seen in Fig. 2 that this turnstile picture of quantum pumping works for all parameter settings by comparing with Fig. 1 (d). As a result of particle-hole symmetry above and below the Dirac point of a potential barrier, transmission probability of the pseudospin-1 Dirac-Weyl fermions demonstrate a sharp V -shape local minimum at the Dirac point. It should be noted that at the Dirac point, eigenspinor wavefunction of the Hamiltonian is ψ_0 and the transmission probability is exactly zero. We singled out this point in all of our calculations. Below the Dirac point, higher potential barriers allow larger transmission probability. Above the Dirac point, higher potential barriers allow smaller transmission

probability. And the difference is very sharp giving rise to a sharp negative pumped current below the Dirac point and a sharp positive pumped current above the Dirac point as shown in Fig. 2 (d). In vast Fermi energy regime, the pumped dc current flows in the same direction for all incident angles as shown in Fig. (a), (b), and (c), giving rise to smooth angle-averaged pumped current shown in Fig. 2 (d). It should also be noted that the sharp current peak close to the Dirac point does not diverge and the current has an exact zero value at the Dirac point by taking into account quasiparticles on the flat band, which is a stationary state while the wavevector in the pump-current direction (x direction in Fig. 1 (a)) is imaginary. The finite value of the pump-current peak is shown in the zoom-in inset of Fig. 4 (d).

The previous discussion is based on the classical turnstile mechanism, while the pumped current is evaluated by the Berry phase of the scattering matrix formed from the parameter variation with a looped trajectory (Eq. (8)). Such a consistency needs further looking into, which is elucidated in the next section.

IV. CONSISTENCY BETWEEN THE TURNSTILE MODEL AND THE BERRY PHASE TREATMENT

In previous literature, consistency between the turnstile model and the Berry phase treatment is discovered while a clear interpretation is lacking.

Berry curvature of the scattering matrix is defined by²

$$\Omega(\alpha) = \sum_{\beta} \text{Im} \frac{\partial s_{\alpha\beta}^*}{\partial V_1} \frac{\partial s_{\alpha\beta}}{\partial V_2}. \quad (10)$$

with the scattering matrix

$$\mathbf{s} = \begin{pmatrix} r & t' \\ t & r' \end{pmatrix}. \quad (11)$$

t/t' and r/r' are the transmission and reflection amplitudes generated by incidence from the left/right reservoir with $t' = t$ and $r' = -r^*t/t^*$.

Without losing generality, we consider a conductor modulated by two oscillating potential barriers $X_1 = V_1$ and $X_2 = V_2$ with the same width and equilibrium height. By defining the modulus and argument of t and r as $t = \rho_t e^{i\phi_t}$ and $r = \rho_r e^{i\phi_r}$ we have

$$\Omega(l) = \sum_{i=t,r} \rho_i \frac{d\rho_i}{dV_1} \frac{d\phi_i}{dV_2} - \rho_i \frac{d\phi_i}{dV_1} \frac{d\rho_i}{dV_2}. \quad (12)$$

We have shown contours of the Berry curvature $\Omega(l)$ and the eight partial derivatives on the right hand side of Eq. (12) in Fig. 3. For convenience of discussion, the parameter space in Fig. 3 (a) to (i) is divided into four blocks. It can be seen from Fig. 3 (a) that $\Omega(l)$ is negative in block II, positive in block III, and nearly zero in blocks I and IV. For the term $\rho_t \frac{d\rho_t}{dV_1} \frac{d\phi_t}{dV_2} - \rho_t \frac{d\phi_t}{dV_1} \frac{d\rho_t}{dV_2}$ in Eq. (12), $\rho_t > 0$, $\frac{d\phi_t}{dV_2} \approx \frac{d\phi_t}{dV_1}$ is negative throughout the four blocks and $\frac{d\rho_t}{dV_1} \approx \frac{d\rho_t}{dV_2}$ is positive in block II and negative in block III (see Fig. 3 (b) and (g)). As a result, this term approximates zero in blocks II and III. For the term $\rho_r \frac{d\rho_r}{dV_1} \frac{d\phi_r}{dV_2} - \rho_r \frac{d\phi_r}{dV_1} \frac{d\rho_r}{dV_2}$ in Eq. (12), $\rho_r > 0$, $\frac{d\phi_r}{dV_2} - \frac{d\phi_r}{dV_1}$ is positive throughout the four blocks (see Fig. 3 (h) and (i)), $\frac{d\rho_r}{dV_1} \approx \frac{d\rho_r}{dV_2}$ is positive in block III and negative in block II. It can also be seen from Fig. 3 that in blocks I and IV the values of the two terms cancel out each other giving rise to nearly zero $\Omega(l)$. Therefore, the combined result of the two terms is that $\Omega(l) > 0$ when $\frac{d\rho_r}{dV_1} > 0$ and $\Omega(l) < 0$ when $\frac{d\rho_r}{dV_1} < 0$. This means that the Berry phase is positive and hence the pumped current is positive when higher potential barrier allows larger reflection probability in block III and that the Berry phase is negative and hence the pump-current direction is reversed when higher potential barrier allows smaller reflection probability in block II. Because $\rho_r^2 + \rho_t^2 = 1$, larger reflection probability means smaller transmission probability, consistence between the Berry phase picture and the classical turnstile model is numerically proved in the pseudospin-1 Dirac-Weyl system.

If we consider normal incidence, consistency between the Berry phase picture and the classic turnstile model becomes straightforward. For normal incidence, derivative of t/r with respect to V_2 is equal to derivative of t'/r' with respect to V_1 . Hence we have

$$\Omega(l) = 2\rho_r \frac{d\rho_r}{dV_1} \left(\frac{d\phi_t}{dV_1} - \frac{d\phi_r}{dV_1} \right). \quad (13)$$

From Fig. 3 we can see that $\frac{d\phi_t}{dV_1} - \frac{d\phi_r}{dV_1}$ is positive throughout the parameter space. Therefore, the Berry phase has the same sign with $\frac{d\rho_r}{dV_1}$, which demonstrates consistency between the Berry phase picture and the classic turnstile mechanism of the adiabatic quantum pumping.

V. CONCLUSIONS

In summary, adiabatic quantum pumping in periodically modulated pseudospin-1 Dirac-Weyl system is studied. By using two ac electric gate-potentials as the driving parameters, direction-reversed pumped current is found by the Berry phase of the scattering matrix at

certain parameter regimes as a result of super Klein tunneling and particle-hole symmetry close to the Dirac point of the band structure. Such a phenomenon originates from the abnormal transmission behavior of the Dirac-Weyl quasiparticles that sometimes they transmit more through a higher electric potential barrier. As a result, definition of the “opening” and “closing” of a gate is reversed in the classic turnstile picture and hence direction of the pumped dc current is reversed. We also provide rigorous proof of the consistency between the quantum Berry phase picture and the classic turnstile mechanism.

VI. ACKNOWLEDGEMENTS

R.Z. is grateful for enlightening discussions with Pak Ming Hui. The work is supported by the National Natural Science Foundation of China (No. 11004063) and the Fundamental Research Funds for the Central Universities, SCUT (No. 2017ZD099).

-
- ¹ D. J. Thouless, Phys. Rev. B **27**, 6083 (1983).
- ² D. Xiao, M.-C. Chang, and Q. Niu, Rev. Mod. Phys. **82**, 1959 (2010).
- ³ M. Switkes, C. M. Marcus, K. Campman, and A. C. Gossard, Science **283**, 1905 (1999).
- ⁴ M. W. Keller, J. M. Martinis, and R. L. Kautz, Phys. Rev. Lett. **80**, 4530 (1998).
- ⁵ L. P. Kouwenhoven, A. T. Johnson, N. C. van der Vaart, C. J. P. M. Harmans, and C. T. Foxon, Phys. Rev. Lett. **67**, 1626 (1991).
- ⁶ R. Zhu and H. Chen, Appl. Phys. Lett. **95**, 122111 (2009).
- ⁷ Y. Wei and J. Wang, Phys. Rev. B **66**, 195419 (2002).
- ⁸ W. Ma, L. Zhou, Q. Zhang, M. Li, C. Cheng, J. Geng, X. Rong, F. Shi, J. Gong, and J. Du, Phys. Rev. Lett. **120**, 120501 (2018).
- ⁹ S. Nakajima, M. Taguchi, T. Kubo, and Y. Tokura, Phys. Rev. B **92**, 195420 (2015).
- ¹⁰ A. Saha, D. Rainis, R. P. Tiwari, and D. Loss, Phys. Rev. B **90**, 035422 (2014).
- ¹¹ M. Alos-Palop, R. P. Tiwari, and M. Blaauboer, Phys. Rev. B **89**, 045307 (2014).
- ¹² R. Zhu and J. Berakdar, Phys. Rev. B **81**, 014403 (2010).
- ¹³ R. Benjamin and C. Benjamin, Phys. Rev. B **69**, 085318 (2004).
- ¹⁴ R. Citro and F. Romeo, Phys. Rev. B **73**, 233304 (2006).
- ¹⁵ F. Romeo and R. Citro, Eur. Phys. J. B **50**, 483 (2006).
- ¹⁶ E. Prada, P. San-Jose, and H. Schomerus, Phys. Rev. B **80**, 245414 (2009).
- ¹⁷ M. Moskalets and M. Büttiker, Phys. Rev. B **66**, 035306 (2002).
- ¹⁸ B. Wang, J. Wang, and H. Guo, Phys. Rev. B **65**, 073306 (2002).
- ¹⁹ B. Wang and J. Wang, Phys. Rev. B **66**, 125310 (2002).
- ²⁰ B. Wang, J. Wang, and H. Guo, Phys. Rev. B **68**, 155326 (2003).
- ²¹ L. Arrachea, Phys. Rev. B **72**, 125349 (2005).
- ²² P. W. Brouwer, Phys. Rev. B **58**, R10135 (1998).
- ²³ B. Bradlyn, J. Cano, Z. Wang, M. G. Vergniory, C. Felser, R. J. Cava, and B. A. Bernevig, Science **353**, 558 (2016).
- ²⁴ M. Orlita, D. Basko, M. Zholudev, F. Teppe, W. Knap, V. Gavrilenko, N. Mikhailov, S. Dvoret-skii, P. Neugebauer, C. Faugeras, A.-L. Barra, and M. Potemski, Nat. Phys. **10**, 233 (2014).
- ²⁵ M. R. Slot, T. S. Gardenier, P. H. Jacobse, G. C. P. van Miert, S. N. Kempkes, S. J. M.

- Zevenhuizen, C. M. Smith, D. Vanmaekelbergh, and I. Swart, *Nature Phys.* **13**, 672 (2017).
- ²⁶ D. Guzmán-Silva, C. Mejía-Cortés, M. A. Bandres, M. C. Rechtsman, S. Weimann, S. Nolte, M. Segev, A. Szameit, and R. A. Vicencio, *New J. Phys.* **16**, 063061 (2014).
- ²⁷ S. Mukherjee, A. Spracklen, D. Choudhury, N. Goldman, P. Öhberg, E. Andersson, R. R. Thomson, *Phys. Rev. Lett.* **114**, 245504 (2015).
- ²⁸ R. A. Vicencio, C. Cantillano, L. Morales-Inostroza, B. Real, C. Mejía-Cortés, S. Weimann, A. Szameit, and M. I. Molina, *Phys. Rev. Lett.* **114**, 245503 (2015).
- ²⁹ F. Diebel, D. Leykam, S. Kroesen, C. Denz, and A. S. Desyatnikov, *Phys. Rev. Lett.* **116**, 183902 (2016).
- ³⁰ W. Beugeling, J. C. Everts, and C. M. Smith, *Phys. Rev. B* **86**, 195129 (2012).
- ³¹ B. Dóra, I. F. Herbut, and R. Moessner *Phys. Rev. B* **90**, 045310 (2014).
- ³² J. D. Malcolm and E. J. Nicol, *Phys. Rev. B* **93**, 165433 (2016).
- ³³ F. Wang and Y. Ran, *Phys. Rev. B* **84**, 241103 (2011).
- ³⁴ M. Tsuchiizu, *Phys. Rev. B* **94**, 195426 (2016).
- ³⁵ H.-Y. Xu and Y.-C. Lai, *Phys. Rev. B* **94**, 165405 (2016).
- ³⁶ A. Fang, Z. Q. Zhang, S. G. Louie, and C. T. Chan, *Phys. Rev. B* **93**, 035422 (2016).
- ³⁷ J. D. Malcolm and E. J. Nicol, *Phys. Rev. B* **90**, 035405 (2014).
- ³⁸ E. Illes, J. P. Carbotte, and E. J. Nicol, *Phys. Rev. B* **92**, 245410 (2015).
- ³⁹ E. Illes and E. J. Nicol, *Phys. Rev. B* **94**, 125435 (2016).
- ⁴⁰ D. J. Griffiths, *Introduction to Quantum Mechanics*, 2nd Ed., Pearson Education Inc. Sec. 4.3, p. 166, (2005).
- ⁴¹ W. Y. Deng, W. Luo, H. Geng, M. N. Chen, L. Sheng, and D. Y. Xing, *New J. Phys.* **17**, 103018 (2015).
- ⁴² M. I. Katsnelson, K. S. Novoselov, and A. K. Geim, *Nat. Phys.* **2**, 620 (2006).
- ⁴³ R. Zhu and P. M. Hui, *Phys. Lett. A* **381**, 1971 (2017).

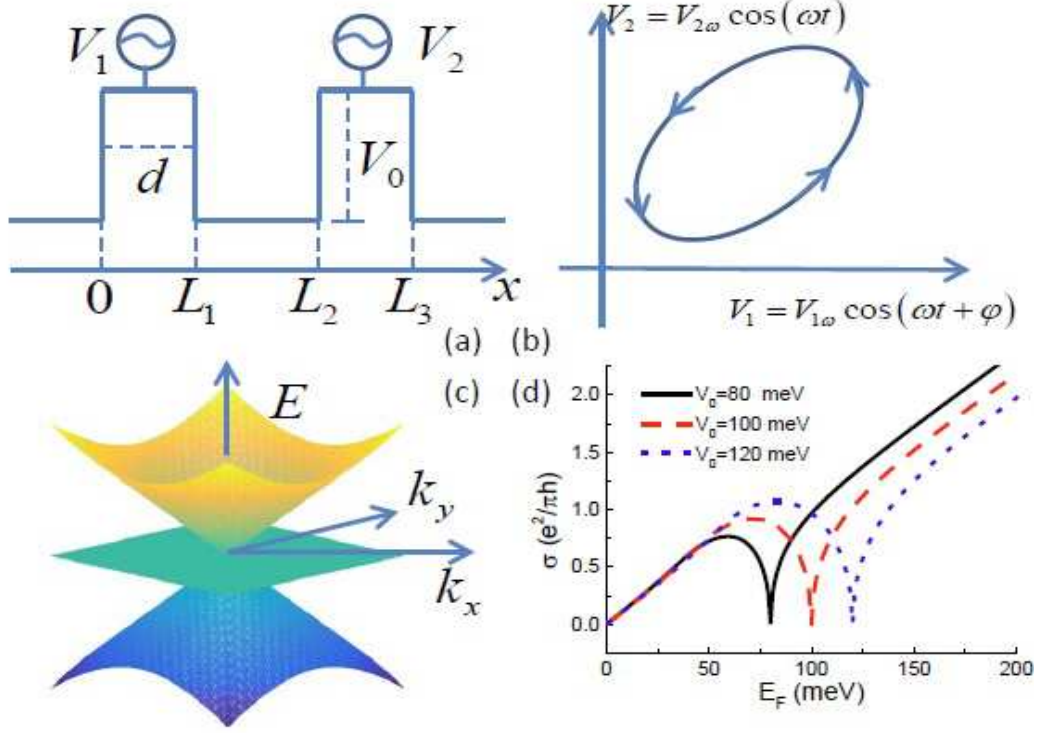


FIG. 1: (a) Schematics of the adiabatic quantum pump. Two time-dependent gate voltages with identical width d and equilibrium strength V_0 are applied to the conductor. Time variation of the two potentials V_1 and V_2 is shown in panel (b). V_1 and V_2 have a phase difference giving rise to a looped trajectory after one driving period. (c) Two-dimensional band structure of the pseudospin-1 Dirac-Weyl fermions with a flat band intersected two Dirac cones at the apexes. (d) Conductivity of the pseudospin-1 Dirac-Weyl fermions measured by $\sigma = \frac{e^2 k_F d}{\pi h} \int_{-\pi/2}^{\pi/2} |t(E_F, \theta)|^2 \cos \theta d\theta$ in single-barrier tunneling junction as a function of the Fermi energy for three different values of barrier height V_0 . $k_F = E_F/\hbar v_g$ is the Fermi wavevector and t is the transmission amplitude defined in Eq. (5). It can be seen that higher barrier allowing larger conductivity occurs at the Dirac point $E_F = V_0$ and around $E_F = V_0/2$ (see the text).

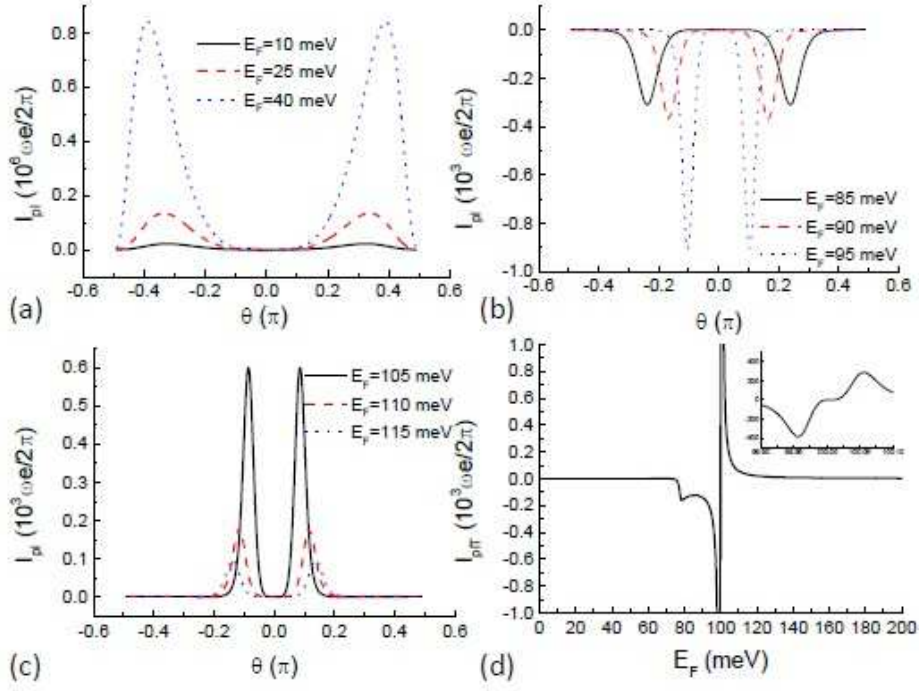


FIG. 2: (a), (b), and (c): Angular dependence of the pumped for different Fermi energies with the driving phase difference φ fixed. (d) Angle-averaged pumped current as a function of the Fermi energy. Its inset is the zoom-in close to the Dirac point to show that the large value of the pumped current does not diverge. Other parameters are $V_0 = 100$ meV, $V_{1\omega} = V_{2\omega} = 0.1$ meV, $d = 5$ nm, $L_2 - L_1 = 10$ nm, and $\varphi = \pi/2$.

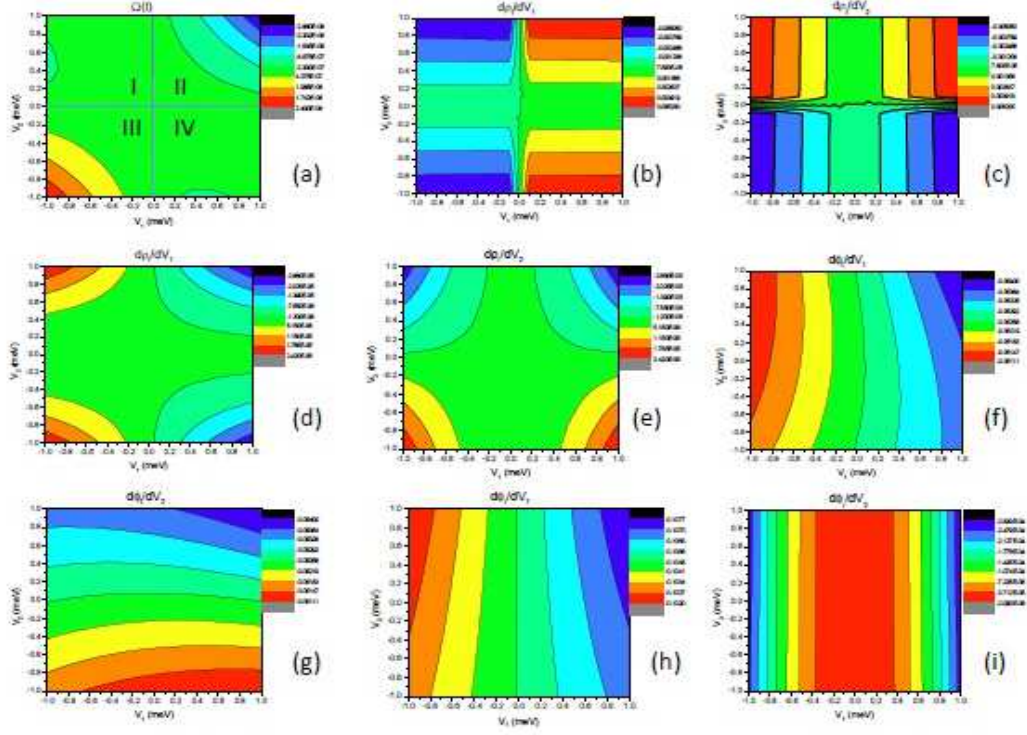


FIG. 3: Contours of the Berry curvature $\Omega(l)$ and the eight derivatives on the right hand side of Eq. (12). Other parameters are $V_0 = 100$ meV, $d = 5$ nm, $L_2 - L_1 = 10$ nm, $E_F = 100$ meV, and $\theta = 0.5$ in radian. For convenience of discussion, the parameter space in the nine panels is divided into four blocks: I ($-1 < V_1 < 0$ and $0 < V_2 < 1$), II ($0 < V_1 < 1$ and $0 < V_2 < 1$), III ($-1 < V_1 < 0$ and $-1 < V_2 < 0$), and IV ($0 < V_1 < 1$ and $-1 < V_2 < 0$). The four blocks are illustrated in panel (a).